UNIVERSITY OF CALIFORNIA SAN DIEGO

Advanced Magnetic Liquid Metal for Printable, Stretchable, and Dynamic Circuits

A Thesis submitted in partial satisfaction of the requirements
for the Master of Science

in

Nanoengineering

by

Mingyao Xu

Committee in charge:

Professor Joseph Wang, Chair
Professor Donald Sirbuly
Professor Sheng Xu

2022

The thesis of Mingyao Xu is approved, and it is acceptable in quality and form for publication on microfilm and electronically.

University of California San Diego

2022

DEDICATION

In recognition of reading this manual before beginning to format the doctoral dissertation or master's thesis; for following the instructions written herein; for consulting with the Graduate Division Academic Affairs Advisers; and for not relying on other completed manuscripts, this manual is dedicated to all graduate students about to complete the doctoral dissertation or master's thesis.

In recognition that this is my one chance to use whichever justification, spacing, writing style, text size, and/or text font that I want to while still keeping my headings and margins consistent.

TABLE OF CONTENTS

LIST OF FIGURES

LIST OF ABBREVIATIONS

EGaIn:	Eutectic Gallium-Indium Alloy (Liquid Metal)
BFC	Biofuel Cell
MLM	Magnetic Liquid Metal
Ni	Nickel
Nd	Neodymium
Nd-Ni MPs	Ferromagnetic Neodymium and Nickel Co-microparticles

ACKNOWLEDGEMENTS

I would like to acknowledge Dr. Joseph Wang for all his support and guidance for being my P.I. and advisor over two years. I would like to acknowledge Cristian Silva Lopez for not only guiding me through the project of smart magnetic liquid metal, but also supporting me in my academia life. I would also like to acknowledge Lu Yin, Zhengxing Li, and Ernesto De La Paz for assisting me in synthesizing the magnetic liquid metal and fabricating biofuel cells.

ABSTRACT OF THE THESIS

Advanced Magnetic Liquid Metal for Printable, Stretchable, and Dynamic Circuits

by

Mingyao Xu

Master of Science in Nanoengineering

University of California San Diego, 2022

Professor Joseph Wang, Chair

Permanent magnetic materials, including cobalt, nickel, iron, and neodymium, have attracted much attention in the last century. These elements are widely used in aerospace engineering, medical services, superconductive material manufacturing, and front research in high-energy physics. Eutectic gallium-indium (EGaIn) is a liquid alloy at room temperature. Due to its high conductivity, low toxicity, and high surface tension, the EGaIn is widely used in research of electrical engineering and thermal materials. However, after combining these two types of materials, we are able to manufacture the liquid metal with an inner magnetic field, which is called the magnetic liquid metal (MLM). To explore and develop its potential

applications, we seek to build functional microstructures and microfluidic channels for stretchable electronics, dynamic circuits, and living actuators.

Chapter 1 is an introduction to ferromagnetic nickel, neodymium microparticles, and the EGaIn. I would like to discuss their physical and chemical properties. Chapter 2 will discuss the synthesis of ferromagnetic materials and the EGaIn, as well as their contribution to potential applications of the MLM. Chapter 3 talks about the fabrication of the dynamic MLM circuit and the examination of its magnetic properties through mechanical, self-healing, and electrochemical tests. Chapter 4 discusses the experiment of integration between the MLM circuit with the biofuel cell (BFC).

In the future, this research would provide a possible strategy for the development of next-generation biosensors or smart bioelectronics, which further enhance people's daily lives and contributes to public health.

CHAPTER 1. INTRODUCTION

1.1 Ferromagnetic materials

As the core knowledge of this project, it is necessary to know the idea of ferromagnetism. Ferromagnetism is defined as the intense attraction between non-electrically charged microparticles. It is associated with nickel, iron, cobalt, and other rare-earth materials. Compared with paramagnetic materials, ferromagnetic materials are easily magnetized and have a higher level of magnetic saturation.

Magnetic properties of magnetic materials originate from the electron states in the d-shells. More unpaired valence electrons lead to better magnetic properties. However, ferromagnetic materials have a more complicated system to generate and maintain magnetic interactions. The ferromagnetic iron could be an excellent example to explain the phenomenon of solid ferromagnetism. From the microscopic perspective, electrons in the 3*d*-shell spin and generate the magnetic dipole momentum, leading to the automatic alignment of atoms and the net magnetic field. From the macroscopic perspective, it is known that electrons are unable to stay in the same position and spin in the same direction due to the Pauli exclusion law. However, the exchange interaction from the electrons in the 4*s*-shell would rotate in the opposite direction, which generates an attractive interaction with the 3*d*-shell electrons and overcomes the repulsive force. As a result, the net interaction between the 3*d*-shell and 4*s*-shell contributes to the overall self-alignment of the 3*d*-shell electrons and further strong ferromagnetism.

1.2 Ferromagnetic Ni microparticles

In nature, nickel (Ni) is the fifth most abundant material. It is widely used in alloy manufacturing and aerospace engineering. Through the electron configuration, Ni has two unpaired electrons in the 3*d*-shell. These two unpaired electrons are parallelly aligned with each other within the magnetic field. As a result, the special electronic configuration offers unique ferromagnetism properties, shielding effect, and high permeability to the Ni microparticles. Generally, the ferromagnetic Ni microparticles have a magnetic saturation of around 0.7 T[1]. Due to the solid ferromagnetic property and high abundance, the ferromagnetic Ni microparticles have a critical role in manufacturing magnetic alloys and electromagnetic shielding devices. To conclude, factors of low price and advanced ferromagnetic properties make ferromagnetic Ni microparticles an ideal material for manufacturing smart, liquid metal-based, and dynamic circuits in this project.

1.3 Ferromagnetic Nd microparticles

Neodymium (Nd), as one of the most robust ferromagnetic materials found in nature, brings us a new strategy to fabricate the smart MLM. Compared with ferromagnetic Ni, Nd has a magnetic saturation of up to 3 T, while ferromagnetic Ni is 0.7 T[1,2,3]. The electron configuration reveals the secret of its ferromagnetism. There are four unpaired electrons aligned in the same direction in 4*s*-shell instead of two in Ni and three in iron. These four free electrons greatly enhance the magnetic properties of Nd, which provides a more significant magnetic dipole moment and high magnetic saturation. The high magnetic saturation ensures the ideal performance of a strong magnetic field and high magnetic coercive force, leading to promising self-healing ability.

1.4 Eutectic gallium-indium alloy

Eutectic gallium-indium (EGaIn, 75 % Ga, 25 % In by weight) is a liquid alloy at room temperature. Due to the properties of low melting point, low resistivity, and low viscosity, people can manipulate its shapes and compositions for different structures while maintaining electrical conductivity. Since the 21st century, EGaIn has attracted much attention in the research of stretchable sensors. People have utilized EGaIn for tunable actuators, stretchable 3D conductors, functional microstructures, and microfluidic channels[4,5,6]. Other factors, including low cost and low toxicity, bring out the vast potential applications of wearable electronics and dynamic circuits.

Research teams had combined permanent magnetic iron (Fe) microparticles with the EGaIn to fabricate ferromagnetic Fe-based magnetic liquid metal. Their work successfully gave out the magnetically induced motion in EGaIn as a conductive and controllable liquid switch. Moreover, another team used the permanent magnetic Ni microparticles to fabricate ferromagnetic Ni-based magnetic liquid metal for a magnetic field-triggered healing ability. They dragged a magnet towards the damaged region to populate it with EGaIn for further healing[7,8]. Although these combinations open a new window for the potential applications, problems of low loading efficiency, poor self-healing ability, and low magnetization properties still limit large-scaled industrial applications and further improvements.

1.5 Construction of a binary co-microparticle system

The ferromagnetic Ni and Nd microparticles would be both used in fabricating MLM. Due to the fascinating magnetic properties of ferromagnetic Nd microparticles, they will become the core material inside the MLM to act as a magnetic field holder. However, it is not easy to

simply mix the ferromagnetic Nd microparticles with the EGaIn to get the MLM we want. Surface tension plays a significant role during the mixing process. Research has been done on the surface tension of ferromagnetic materials and EGaIn. EGaIn has a surface tension of 1.6 N m^{-1} instead of 1.900 N m^{-1} in ferromagnetic Ni microparticles and 0.5 N m^{-1} in ferromagnetic Nd microparticles. The high surface tension of the EGaIn will prevent the well-mixing between the EGaIn and ferromagnetic particles. The strategy for solving the issue is introducing the ferromagnet Ni microparticles as a binder. The higher surface tension of Ni microparticles will promote particle submerging. As a result, the ferromagnetic Ni microparticles act as a perfect mediator to load the ferromagnetic Nd microparticles into the EGaIn.

The ferromagnetic Nd microparticles could incorporate with the ferromagnetic Ni microparticles under a solid magnet to form a “host-and-guest” relationship. Due to the permanent magnetic property, this relationship could generate stable neodymium-nickel co-microparticles (Nd-Ni MPs) as the most significant loading materials inside the EGaIn. The Nd-Ni MPs could be a promising candidate for constructing a new “magnetic bridge” inside the EGaIn, which serves for further applications.

CHAPTER 2. MATERIAL SYNTHESIS

2.1 Fabrication of MLM

The ferromagnetic microparticles were prepared separately. Nd-based magnet blocks were crushed and later filtered with a metal mesh. The metal mesh had a hole size of 177 microns, which allowed us to maintain homogeneity of the particle size for ferromagnetic Nd microparticles. The EGaIn was prepared by adding 75 g of gallium blocks and 25 g of indium chunks. The mixture was heated to 120°C and stirred for 4 hours. The alloy was cooled overnight at room temperature for further fabrication of MLM. Quantified ferromagnetic Ni (Sigma-Alrich, Saint Louis, MO) and Nd microparticles, with a weight ratio of 1:1, were weighed and mixed in the strong magnetic field for binding and magnetization. The co-microparticles were transferred to the EGaIn and stirred for 10 minutes.

2.2 Characterization of MLM

2.2.1 Surface morphology synthesis

The scanning electron microscopy (Philips XL30 ESEM) was used to characterize the surface morphology of co-microparticles and EGaIn. As shown in figure 1, the Ni microparticles were spherical, while rectangular for Nd microparticles. The left bottom figure displayed the homogeneity of particle size in the range of 100 to 150 μm, which successfully demonstrated Nd microparticles' previous size-controlled grounding and filtration. By comparing the SEM images of pure Ni microparticles and Nd microparticles, it was also found that Ni microparticles had a rougher surface than that of Nd microparticles. It could be believed that the coarse surface morphology of Ni microparticles contributed to adhesion between the EGaIn, Nd microparticles and the whole further stability of the MLM system. The middle figure was the co-microparticles after magnetization. The ferromagnetic Ni microparticles tightly bonded to the Nd

microparticles, forming a mediator layer for further aggregation. Figure 1 (right) was the sample of MLM. A smooth and homogeneous layer of EGaIn lay on the co-microparticles. It proved that the ferromagnetic Ni microparticles did play a significant role in binding.

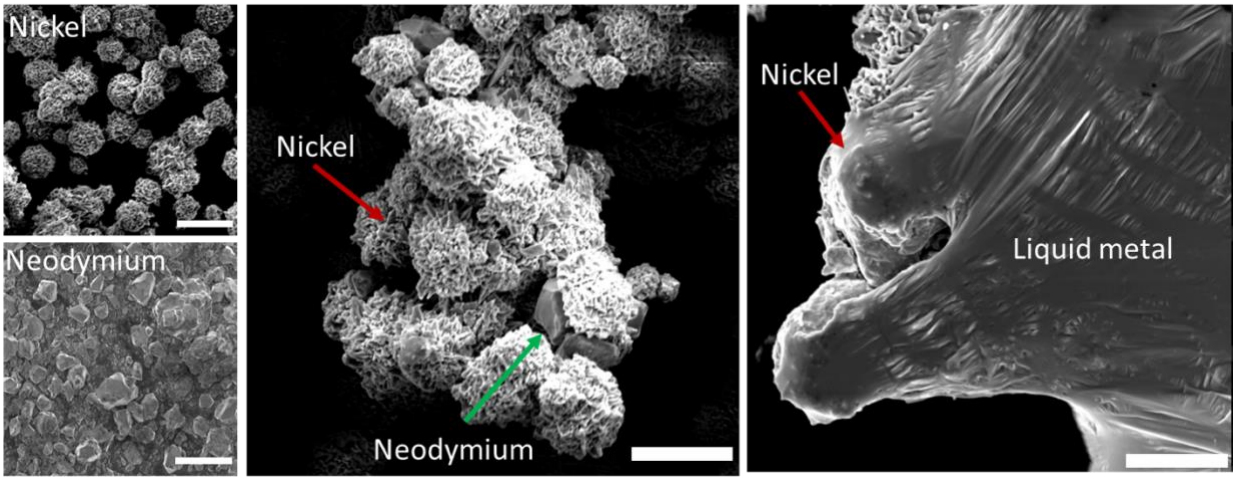

Figure 1. SEM images for Ni microparticles (left top), Nd microparticles (left bottom), Nd-Ni MPs (middle), and MLM (right).

2.2.2 Quantitative loading synthesis

To reach the best loading efficiency (wt %/V) and mechanical properties, different amounts of ferromagnetic particles were loaded into the EGaIn. Figure 2 gives a macroscopic review of the MLM with varying loading materials. MLM reacted differently to the magnetic field with different loading efficiency. With the increment of loading materials, the MLM was more and more sensitive to the magnetic field. However, it gradually lost the properties of water and became more pristine.

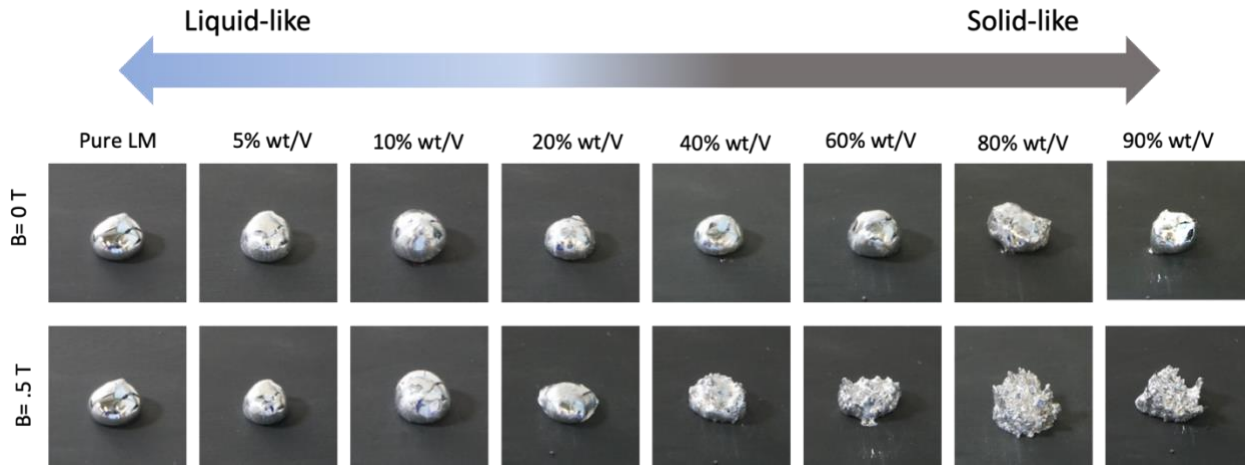

Figure 2. The LML with different loading efficiency.

Conductivity, resistance, and strain were measured in each sample of MLM. As shown in figure 3, the conductivity linearly increased with increasing amounts of loading materials. Figure 3 (right) displays the relationship between the change of resistance and strain. It was found that the higher the loading efficiency, the more sensitivity of resistance changes towards increasing pressure. Based on different samples' macroscopic and physical analysis, we could conclude that more loading materials do not necessarily mean better performance. With the increment of loading amounts, the MLM behaves more like a solid, opposite to what we want as a ferrofluid. To earn a balance between the physical performance and the properties of maintaining as a liquid, we finally chose the loading efficiency at 60% to continue our experiment and synthesis.

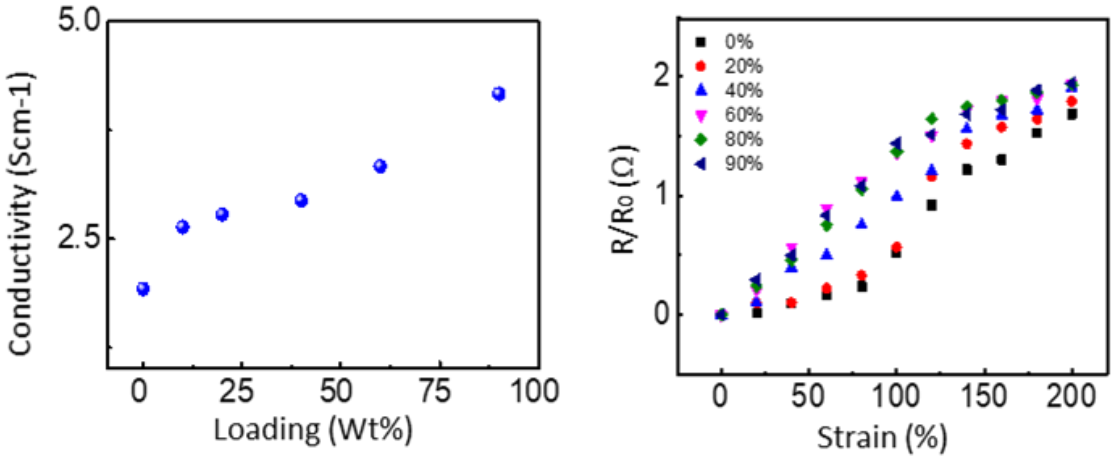

Figure 3. Conductivity (left), resistance, and strain (right) to different loading efficiency.

2.2.3 Magnetic synthesis

Magnetic properties of the sample with 60% loading efficiency were measured and compared with those that did not contain ferromagnetic Nd microparticles. A series of magnetization and demagnetization processes was conducted to calculate the magnetic hysteresis of samples with 60% loading efficiency and only with ferromagnetic Ni microparticles. As shown in figure 4, the magnetic hysteresis was greatly enhanced with the addition of ferromagnetic Nd microparticles. It was not hard to understand that as the core materials, ferromagnetic Nd microparticles played an essential role in maintaining the magnetic performance of our MLM. The magnetic moment was also measured. It was observed that the magnetic moment of the sample loaded with ferromagnetic Nd microparticles was much higher than only loaded with ferromagnetic Ni microparticles. The magnetic hysteresis and moment measurements illustrated that the MLM loaded with 60% of Nd-Ni MPs could be an ideal material for further construction of MLM-based bioelectronics with fascinating mechanical properties and healing abilities

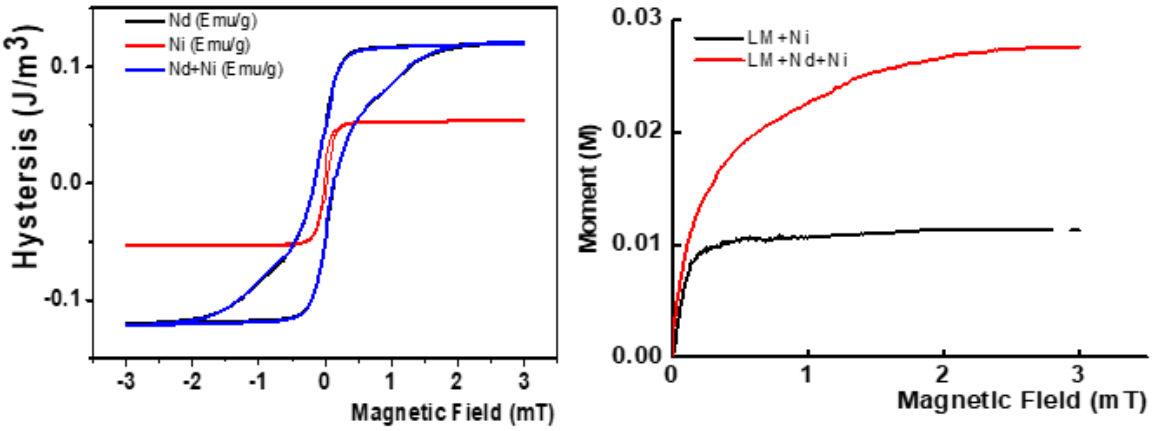

Figure 4. Magnetic hysteresis (Left) and moment (Right) for MLM sample with 60% loading efficiency.

ACKNOWLEDGE

Chapter 2, in full, is currently being prepared for submission for publication of the material. Mingyao Xu; Cristian Silva Lopez. The thesis author was the primary researcher and author of this material.

CHAPTER 3. EXPERIMENT AND SYNTHESIS

3.1 Fabrication of MLM circuits

Based on the previous synthesis of magnetic properties and macroscopic evaluation, the MLM with 60% loading efficiency provided us with excellent performance. The following experiments shall all use this MLM for fabricating MLM circuits.

Styrene-Ethylene-Butylene-Styrene-Thermoplastic Elastomer (SEBS-1645) particles were dissolved in dichlorobenzene with a mass ratio of 4:10 to obtain the sigma SEBS resin with desired viscosity. 2g of water-based polyurethane (PU) resin was mixed with 100 mg of crosslinker to get the PU resin with appropriate viscosity. Stretchable textile (Lycra Shiny Milliskin Nylon Spandex) was prepared as the substrate for constructing MLM circuits.

The first layer of SEBS was printed on the stretchable textile with a metal scratch to achieve a smooth surface. The fabric was then heated to 60°C for 20 minutes. After cooling at room temperature, we painted the second layer of PU on the SEBS layer to increase the adhesion between the MLM circuit and the SEBS layer (also the textile). The fabric was transferred to the oven for another heat treatment at 65°C for 15 minutes. After cooling, the well-modified MLM was transferred onto the textile with a plastic mask. A magnet was placed below the substrate to align the MLM and stabilize its shape fully.

3.2 Mechanical Synthesis and Self-healing Test

The well-developed MLM circuit was evaluated using a series of high-speed, high-strains, and cyclic stretching tests. Two heading of the substrate were attached to the electromotor for 25%, 50%, and 100% strain-stretching with a steady speed of 2 cm s^{-1}. This experiment could test the stability of the whole stretchable system of the MLM circuit and the mechanical behaviors of the MLM circuit while facing external stress.

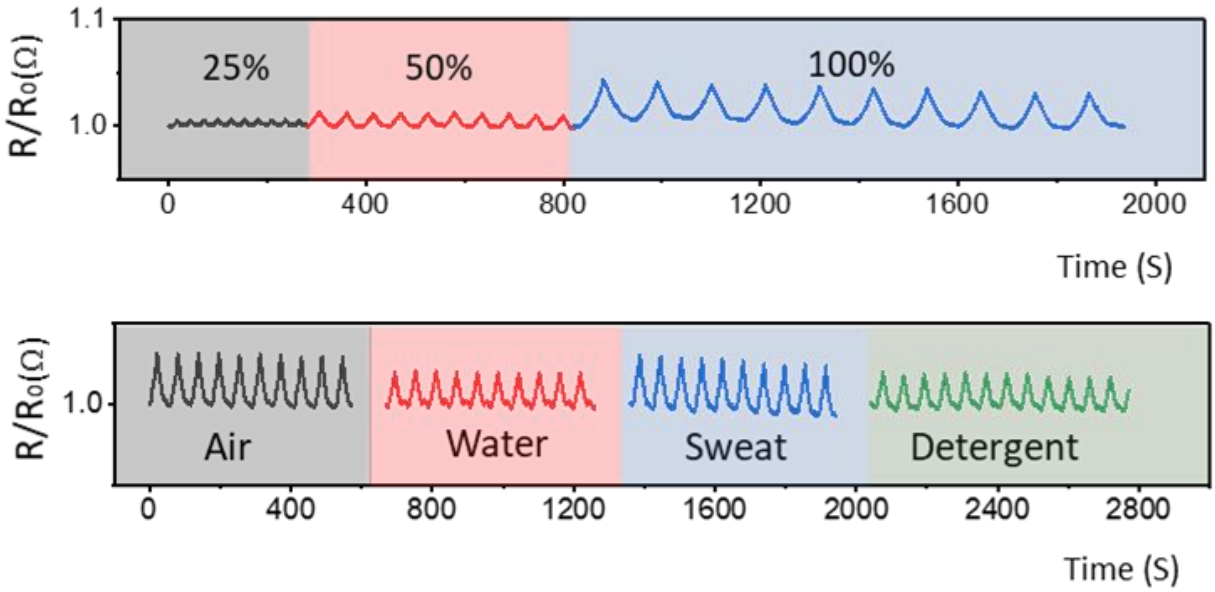

Figure 5. Cyclic stretching (top) and environmental test (bottom).

As shown in figure 5 (top), continuous stretching was conducted. The stretchable MLM circuit was undergoing steady stretching with three different lengths. A noticeable accumulation of microscopic fatigue could be observed in changing resistance during each cycle, especially for the strain of 100%. However, the MLM circuit still held the microscopic deformation between ferromagnetic microparticles and EGaIn. The whole structure was preserved as its original design for falling resistance after retaining initial strains. DI water, sweat solution, and detergent solution were used to stimulate harsh environments that the MLM circuit might encounter under working conditions. 5 mL of each solution was pipetted on the MLM circuits at the beginning of 100% strain-stretching with a steady speed of 2 cm s^{-1}. As illustrated in figure 5 (bottom), these different solutions did not prohibit the normal function of the MLM circuits. We could conclude that the well-constructed MLM circuit can work as a dynamic conductor while facing harsh environments or severe mechanical deformation.

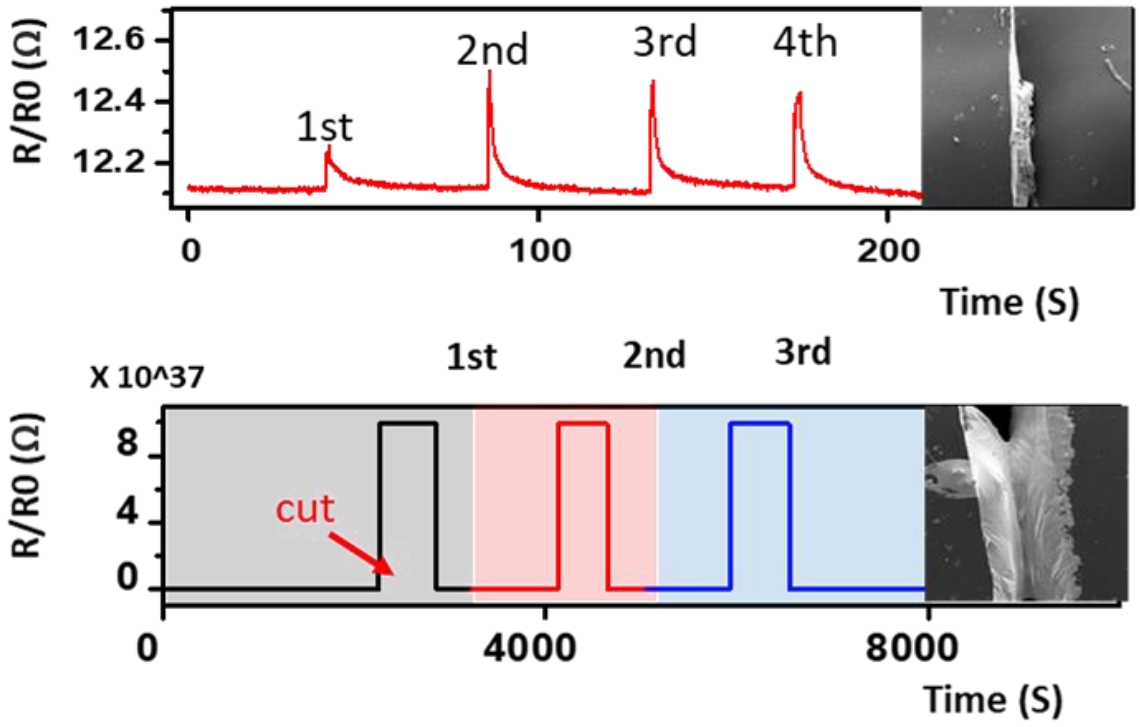

Figure 6. Continuous scratching (top) and repeated cracking (bottom) of MLM circuits.

One primary purpose of this project was to fabricate innovative MLM circuits with self-healing ability. Thus, recording and analyzing the time-dependent self-healing after damage would be appropriate to examine our MLM dynamic circuits. Different types of damage, including scratching and cracking, were applied to the surface of the circuit. A cutting blade was used to damage the circuit surface for a shallow disruption for the scratching during a deep and complete disruption for the cracking. As shown in figure 6 (top), four continuous scratching was made while measuring the resistance. A sharp increase in the resistance could be observed when a scrape happened. However, the resistance did not permanently maintain a high value. The SEM image demonstrated our hypothesis of healing for shallow scratching. The solid co-microparticles were not affected by scratching. They remained in their original positions and

magnetic binding. The EGaIn flew out of the damaged surface within one second to realize the self-healing. For the scenario of cracking, the MLM circuit was separated completely for widths of 1 mm, 3 mm, and 5mm. As expected, the MLM circuit was able to recover its conductivity. As shown in figure 6 (bottom), the SEM image of the cross-section demonstrated the mechanism behind self-healing. While encountering macroscopic disconnections, the inner magnetic field between ferromagnetic co-microparticles would drive the EGaIn as a ferroliquid to realize the self-healing.

3.3 Electrochemical Synthesis

Mechanical tests provided a more macroscopic perspective to evaluate the self-healing ability of our MLM circuit. From a microscopic view, it is necessary to process cyclic voltammetry (CV) studies for electron transformation as MLM bridge deformation and recombination feedback. In addition, the CV study could also provide real-time screening for the electrochemical performance of the MLM circuit during deformation or receiving damage. The potentiostat (CHI 660C, Austin, TX) was used to measure the voltammograms with a scan rate of 5 mV/s. To control the consistency of experiments, we prepared the same MLM circuit as what we did in previous mechanical tests. We ran the cyclic strain-stretching up to 100 % for five cycles to analyze the electrochemical properties of our MLM circuit. As shown in figure 7 (left), the oxidation and reduction peak potentials do not shift during stretching, which improves the stability of MLM while facing external stress.

Furthermore, three repeated scratching were also performed along the circuit, which was the same as we did in section 2.2. Figure 7 (right) shows that the induced current immediately gave out unstable feedback when the damage happened. However, within a few seconds, the inner magnetic field-driven healing stopped the scratching parts and began to recombine the

damaged circuit. After the self-healing process, the circuit maintained its function in its original condition until the subsequent scratching.

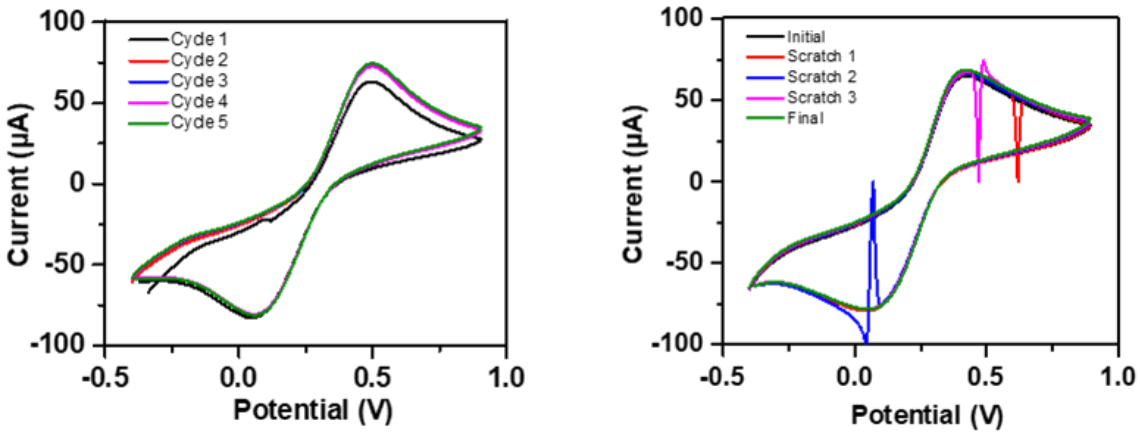

Figure 7. CV plots for stretching trace (left) and scratch-healing trace (right).

ACKNOWLEDGE

Chapter 3, in full, is currently being prepared for submission for publication of the material. Mingyao Xu; Cristian Silva Lopez. The thesis author was the primary researcher and author of this material.

CHAPTER 4. INTEGRATED SYSTEM BETWEEN MLM CIRCUIT AND BFC

4.1 Background to bioelectronics

Was known that the first bioelectronic experiment was conducted by Luigi Galvani in the 18th century, who twitched the detached legs of a frog after applying a small voltage[9,10]. Galvani's experiment could be seen as the genesis of bioelectronics. The word "Bioelectronics" appeared in the mid-1990s when scientists tried to shrink the size of medical devices and monitor human organs efficiently. Heading to the 21st century, the development of bioelectronics enters a new era, which displays unlimited possibilities in environmental protection, health monitoring, and human-biological research. Nowadays, people like to refer the bioelectronics as the dynamic and systemic analysis of the human body via functional biological materials or biological architectures.

Advanced bioelectronics has opened fascinating opportunities for modern biomedical applications, including fields of point-to-point healthcare, energy storage, and hazard detection. Biosensors, including glucose biosensors, DNA-based nanosensors, and enzyme-based biosensors, have successfully demonstrated their precise detection ability. However, these smart sensors are vulnerable to different working conditions. Problems of unstable signal generation, low lifespan, weak damage resistance, limited self-sustainability, and poor mechanical properties become significant obstacles that limit new-gen developments. People have made tremendous efforts into microscopic enhancement for bioelectronics. For instance, research teams integrate nanoparticles, including silver, gold, etc., to improve signal generation. Also, teams are using conducting polymers to retain the stability of electronic signals[10]. However, not much effort has

been put into macroscopic protection. Physical drawbacks are still limiting the widespread application of intelligent bioelectronics. Urgent solutions should be taken to overcome these problems[11].

Here, we propose fabricating the dynamic MLM circuit, which acts as a solid base for further incorporation with functional bioelectronics. As described, with the involvement of ferromagnetic Nd microparticles cooperating with the ferromagnetic Ni microparticles inside the EGaIn, Nd-Ni MPs become the core loading material to bring out better mechanical, magnetic, and physical properties. The well-modified MLM circuit could be a possible strategy to enhance sustainability and self-healing abilities significantly. Once the circuit gets damaged, the strong magnetic attraction between the Nd-Ni MPs begins to move towards each other. The inner magnetic field will drag the EGaIn moving forward and finally realize the spontaneous recombination of cracking parts. As a result, the dynamic MLM circuit could be one solid protection against physical damages applied to bioelectronics.

4.2 Dynamic circuit design and integration with BFC

In order to fully realize the potential of our MLM circuit, it needs to be integrated into a bioelectronic device prototype for a particular situation. To be inspired by the recent development of wearable bioelectronic devices in 2018 by Lv, Jian, et al.[12], we shall utilize their principles of fabricating BFC as an integration strategy in the following experiments. In the original paper, the research team manufactured a wearable textile-based supercapacitor–biofuel cell (SC–BFC) system. The BFC would scavenge energy from enzymatic reactions of lactose from sweat, which was then stored in a super-capacitor (SC) as electrical energy. The BFC and

the SC were integrated on two sides of the conductive and wearable fabric to form a fully functional device.

Because of the stretching, twisting, and all the other forms of stress present in textile materials, the devices, and circuitry within the device need to be capable of withstanding the external stimuli. In the example device, the silver circuit material was printed in a twisting shape to mitigate the stress on the materials themselves, which is where we can integrate liquid metal circuits. As we introduced earlier, the EGaIn has self-healing abilities using the internal magnetic attraction of its co-microparticles. It will reform the circuit even if it is damaged under stress, offering itself as the optimal material as the current collector for wearable biodevices to replace the silver current collector in the previous example.

In a similar setup as Lv's work[12], we would like to the EGaIn as the circuit media for the BFC using the same principles and textile-polymer substrate. The BFC itself is sufficient to be used as a power source for a biosensor to detect various substances like blood alcohol content. As mentioned earlier, the BFC component uses the enzyme lactate oxidase and the redox mediator naphthoquinone (NQ) to facilitate lactate oxidation, forming pyruvate. The carbon layer then collects the lost electron and passes it onto the liquid metal circuit. The cathodic reaction of this fuel cell comes from the reduction of Ag_2O to Ag. Both the bio-anode and the bio-cathode would be in direct contact with the skin to harvest the energy. This energy will be used to support a low-power wearable sensor on the same textile piece. Its current collector and circuitry will also be based on liquid metal. We can conduct experiments verifying its sensory response under different skin conditions and its self-healing capabilities under lateral and rotational stress.

To create a dynamic circuit, we first designed the outline of the MLM-based circuit. As shown in figure 8, the stretchable nylon textile was used as the substrate for the MLM circuit. The textile was first coated with the PU layer. It was then baked for 30 minutes at 50°C. After cooling, another layer of sigma SEBS was painted on the PU layer. Similarly, the painted substrate was baked for another 30 minutes at 50°C. The combination of the PU layer and SEBS layer contributed to maintaining the thermostability, flexibility, and attachment between the MLM circuit and the textile. The "UC" shaped MLM circuit is printed by placing a mask made of plastic paper. A magnet was placed below the substrate for guided printing and fully aligned ferromagnetic co-microparticles.

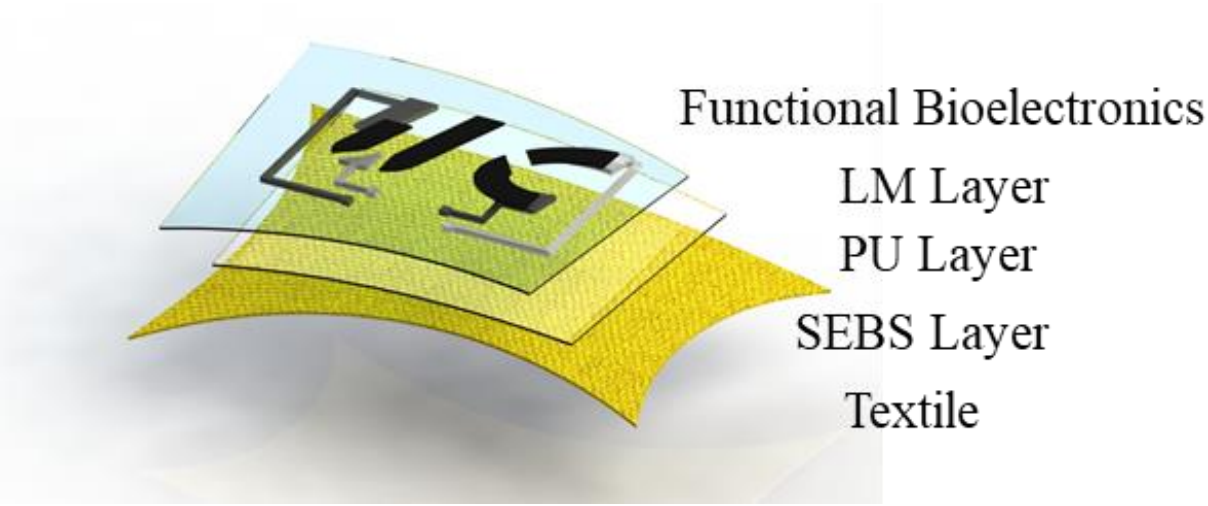

Figure 8. Schematic design of MLM-based dynamic circuit.

4.3 Biofuel cell design

As shown in Figure 9, we designed the BFC with a layer-by-layer structure. There were two components inside it, one was the bio-cathode, and another was the bio-anode. The bio-cathode played a significant role in the enzymatic reduction reaction. At the same time, the bio-

anode operated the enzymatic oxidation in the presence of human sweat or other human body fluids. We shall talk about detailed fabrication processes for the bio-cathode and bio-anode.

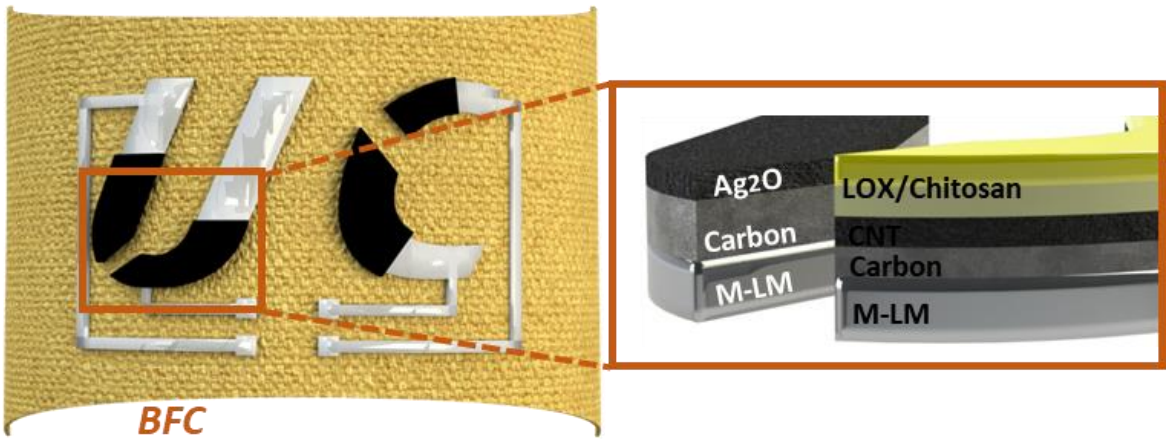

Figure 9. Schematic of BFC.

4.3.1 Bio-anode assembly

The bio-anode was constructed with additional two layers followed by a final functional layer through drop-casting of enzyme solutions. The first layer is the current collector layer made of stretchable carbon ink. 10 mg of oxidized multi-walled carbon nanotubes (MWCNTs-COOH), 30 mg of superconductive carbon & graphite (Super-P), and 100 mg of graphite were mixed with 500 mg of Sigma SEBS. The mixture was stirred for 30 minutes. After painting, the substrate was baked at 65°C for 15 minutes. After cooling, we painted the second cover layer on the current collector layer as a stabilizer between the functional layer and the base circuit. 30 mg of oxidized MWCNTs, 60 mg of Super-P, and 90 mg of graphite were mixed with 300 mg of sigma SEBS by stirring for another 30 minutes. Similarly, the substrate was baked at 65°C for 15 minutes and waited to cool at room temperature.

The functional layer was referred to as the enzymatic layer, which played an essential role in the BFC charging. To anchor enzymes on the top, several drop-casting processes were followed by four steps of drop-casting. In the first step, 2 mg of MWCNTs was added to 0.2 M NQ mediator, and the mixture was then mixed with 30 μL of ethanol/acetone solution with a volume ratio of 9:1. The solution was drop-casted on the coverage layer with 6 μL every 10 minutes. In the second step, 20 mg mL^{-1} lactate oxidase (LOx) and 10 mg/mL bovine serum albumin (BSA) were mixed to make 40 μL of mediator solution. The second drop-casting was taken with 10 μL every 10 minutes. For the third step, 30 step μL of 1% glutaraldehyde solution was drop-casted on the surface with 6 μL every 10 minutes. Finally, 40 μL of 1 wt% chitosan and 10 μL of 0.1 M acetic acid were mixed for drop-casting with 10 μL every 10 minutes as forming the protection layer. During each step of drop-casting, we waited about 30 to 60 minutes to ensure the complete drying of previous layers. The finished bio-cathode was stored in the freighter at 14°C overnight for further testing. Each drop-casting step was performed after the previous casted solution had completely dried at room temperature. The chitosan layer was left to dry overnight.

4.3.2 Bio-cathode assembly

The bio-cathode was constructed with two additional layers. The first layer was the stretchable carbon ink, the same as we used in building the first layer for the bio-anode. The substrate is then baked at 65°C for 10 minutes and cooled at room temperature.

The second layer was constructed with silver oxide and MWCNTs as the active electrode. 11.25 mg of Ag_2O and 3.75 mg of MWCNTs were stirred with 50% ethanol for preparing 500 μL of 30 mg mL^{-1} drop-casting solution with the addition of Nafion solution (25 μL) as the stabilizer. The bio-anode was drop-casted with 30 μL every 5 minutes. The finished bio-anode

was also stored in the freighter at 14°C overnight for further testing. As shown in Figure 10, it was the actual image of the wearable BFC after assembling.

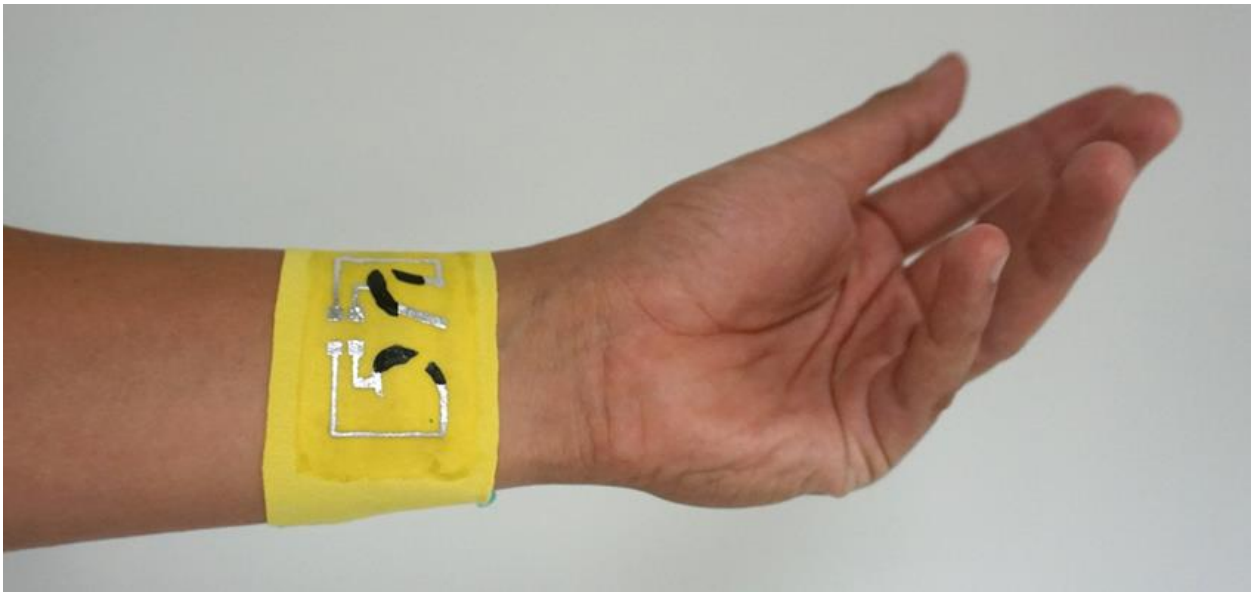

Figure 10. A general overview of BFC on MLM circuit.

4.4 Electrochemical test

The electrochemical performance of the BFC was conducted with the μAUTOLABIII impedance analyzer by measuring the open circuit voltage (OCV). The finished BFC was brought from the freighter and rested at room temperature for 10 minutes. The geometrical area of the BFC was measured, at approximately 1 cm^2, for further calculation of power density. To qualify the electrochemical performance of the BFC, 200 μL of 0.5 M phosphate buffer solution (PBS) was added to the conjunction between the bio-anode and the bio-cathode. 5 μL of 5 mM lactate solution was added to the PBS to stimulate the human sweat in the range of 0 to 30 mM.

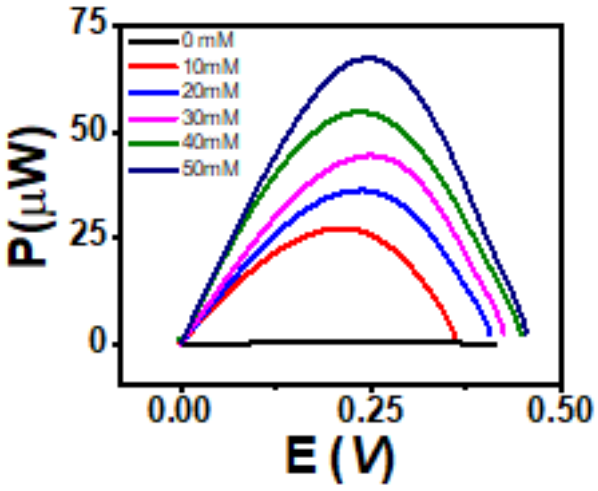

Figure 11. Power density versus voltage at different lactate concentrations.

We tested the power output under the unit area by stimulating the environment of human sweat. As shown in figure 11, the power density reaches its maximum point at 70 μW cm^{-2} when the concentration of lactate is 50 mM, reflecting a good performance of lactate oxidation and energy harvesting.

4.5 Mechanical test

To test the mechanical stability of the BFC, we ran a series of stretching and bending tests to evaluate the mechanical performance of the BFC. Figure 12 (left and middle) shows that we ran the stretching test up to 25% with 25 circles. After the stretching test, we ran another bending test for 25 circles. With the incorporation of SEBS/PU binary attachment, resilience could be dissipated through the binary polymer structure. As shown in figure 12 (right), the BFC was found to uphold the mechanical stability and suitable attachment to the textile. There were no cracks and deformation of the BFC functional layer and the MLM dynamic circuit.

Figure 12. Stretching test (left), bending test(middle), and the Rest (right).

The final test was to demonstrate the self-healing ability against damages or cracks. As shown in figure 13, a small knife was used to cut the MLM dynamic circuit. The crack was 3 cm long and 0.1 cm deep. The crack was made after the first cycle of the OCV as the continuous power output test while encountering physical damage.

Figure 13. Man-made Crack on MLM Dynamic Circuit.

After applying the physical crack, we kept running the OCV test. It was found that the ferromagnetic materials inside the EGaIn played a significant and successful role in prompting self-healing. As previously mentioned, the inner magnetic fields inside ferromagnet co-microparticles were able to recombine after separation. The movement of these co-microparticles

would drive the flow of EGaIn, which realizes the final reconstruction of the pathway. Figure 14 proves the idea of self-healing. The left figure displays an unchanged power output after receiving the physical crack. The right figure shows a steep increment of resistance, which represents the presence of damage. However, the healing did not last too long. Within one second, the MLM dynamic circuit realized the healing. After recovery, the cracked parts did not have any disconnection, and it successfully held the circuit as a “permanent glue.”

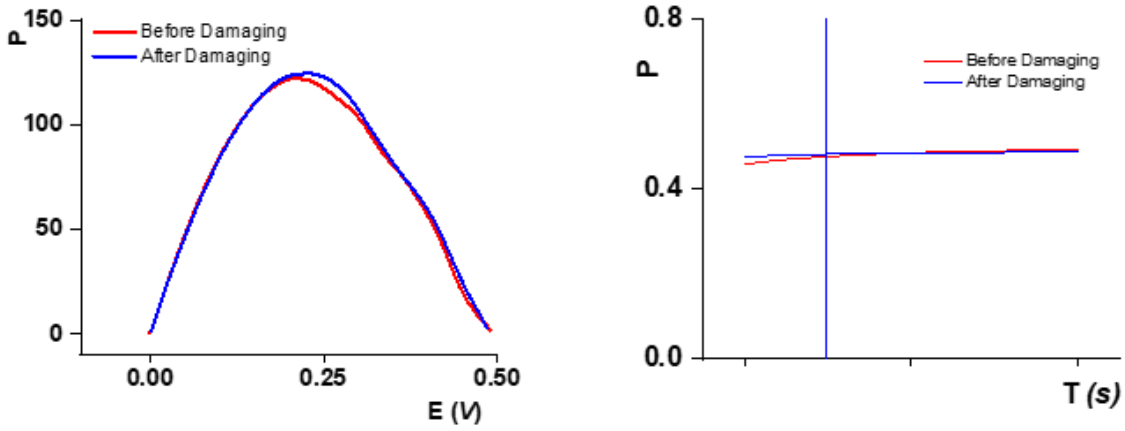

Figure 14.Power output test before and after damaging (left), resistance before and after damaging (right).

ACKNOWLEDGE

Chapter 4, in full, is currently being prepared for submission for publication of the material. Mingyao Xu; Cristian Silva Lopez. The thesis author was the primary researcher and author of this material.

CHAPTER 5. CONCLUSION

Our approach to the new design of a wearable MLM circuit would open a novel strategy to incorporate inorganic nanomaterials with enzyme-based biomaterials for well-development bioelectronics. Our study for integrating the MLM dynamic circuit and BFC successfully demonstrates the possibility of fabricating the MLM-BFC hybrid system. This system has great potential as the foundation for the further combination of other smart bioelectronics. The incorporation between the well-modified MLM-BFC and other micro-bioelectronic devices could build an efficient and stable path for self-sustained micro-detection and micro-controlling in biomedical fields.

To fully develop the feasibility of this study. Systematical synthesis and modification still need to be taken for careful adjustment of MLM ingredients and BFC fabrication. These steps could ensure excellent performance of the basic circuit and integrated BFC. Unfortunately, due to lack of time and adequate funding, tasks, including enhancing material loading efficiency, increasing power density, and improving self-healing ability, should be done before industrial applications and massive production.

The goal of this project was to offer an understanding of potentials for the MLM and further investigations of soft electronics. As a result, not only in the engineering fields but also in people's daily lives, this technology could be functionalized. By achieving that, we hope it can further contribute to public health.

REFERENCES

[1]Lu, H. M., W. T. Zheng, and Q. Jiang. "Saturation magnetization of ferromagnetic and ferrimagnetic nanocrystals at room temperature." *Journal of Physics D: Applied Physics* 40.2 (2007): 320.

[2]S. Magdaleno-Adame, G. J. Cunningham, D. Miller and S. O'Brien, "Calculation of the Remnant Magnetization and Magnetic Saturation Characteristics for Sintered NdFeB Permanent Magnets Utilizing Finite Element Transient Simulations," in *IEEE Transactions on Magnetics*, vol. 55, no. 12, pp. 1-9, Dec. 2019, Art no. 2101909, doi: 10.1109/TMAG.2019.2940426.

[3]Crangle, J., and G. M. Goodman. "The magnetization of pure iron and nickel." *Proceedings of the Royal Society of London. A. Mathematical and Physical Sciences* 321.1547 (1971): 477-491.

[4]Boley, J. William, Edward L. White, George T-C. Chiu, and Rebecca K. Kramer. "Direct writing of gallium-indium alloy for stretchable electronics." *Advanced Functional Materials* 24, no. 23 (2014): 3501-3507.

[5]So, Ju-Hee, Jacob Thelen, Amit Qusba, Gerard J. Hayes, Gianluca Lazzi, and Michael D. Dickey. "Reversibly deformable and mechanically tunable fluidic antennas." *Advanced Functional Materials* 19, no. 22 (2009): 3632-3637.

[6]Park, Junyong, Shuodao Wang, Ming Li, Changui Ahn, Jerome K. Hyun, Dong Seok Kim, Do Kyung Kim, John A. Rogers, Yonggang Huang, and Seokwoo Jeon. "Three-dimensional nanonetworks for giant stretchability in dielectrics and conductors." *Nature communications* 3, no. 1 (2012): 1-8.

[7]Hu, Liang, Hongzhang Wang, Xiaofei Wang, Xiao Liu, Jiarui Guo, and Jing Liu. "Magnetic liquid metals manipulated in the three-dimensional free space." *ACS applied materials & interfaces* 11, no. 8 (2019): 8685-8692.

[8]Guo, Rui, Xuyang Sun, Bo Yuan, Hongzhang Wang, and Jing Liu. "Magnetic liquid metal (Fe-EGaIn) based multifunctional electronics for remote self-healing materials, degradable electronics, and thermal transfer printing." *Advanced Science* 6, no. 20 (2019): 1901478.

[9]Rivnay, Jonathan, Róisín M. Owens, and George G. Malliaras. "The rise of organic bioelectronics." *Chemistry of Materials* 26, no. 1 (2014): 679-685.

[10]Vitale, Flavia, and Brian Litt. "Bioelectronics: the promise of leveraging the body's circuitry to treat disease." *Bioelectronics in Medicine* 1, no. 1 (2018): 3-7.

[11]Goode, J. A., J. V. H. Rushworth, and P. A. Millner. "Biosensor regeneration: a review of common techniques and outcomes." *Langmuir* 31, no. 23 (2015): 6267-6276.

[12]Lv, J., Jeerapan, I., Tehrani, F., Yin, L., Silva-Lopez, C.A., Jang, J.H., Joshuia, D., Shah, R., Liang, Y., Xie, L. and Soto, F., 2018. Sweat-based wearable energy harvesting-storage hybrid textile devices. *Energy & Environmental Science*, *11*(12), pp.3431-3442.